A TIME-EXPLICIT IMMERSED BOUNDARY PROJECTION METHOD FOR THIN ELASTIC SURFACES AND STATIONARY BODIES

BY

NOAH OSMAN

THESIS

Submitted in partial fulfillment of the requirements
for the degree of Master of Science in Aerospace Engineering
in the Graduate College of the
University of Illinois Urbana-Champaign, 2021

Urbana, Illinois

Advisor:

Assistant Professor Andres Goza

Abstract

We present an immersed-boundary method for flows around either an arbitrary body undergoing prescribed kinematics, or a thin elastic body whose motion is fully coupled to the flow dynamics (i.e., involving fully coupled fluid-structure interaction, FSI). The key novelty here is that the proposed method uses an explicit time integration approach (via a Runge-Kutta-Chebyshev framework) for the stiff diffusive term while retaining a formal projection formulation to ensure that the no-slip boundary condition is exactly satisfied to within machine precision at each time instance. The explicit treatment of the diffusive term avoids the embedded large linear solves that plague the majority of fractional step formulations for incompressible flows, while the projection formulation avoids the use of heuristic parameters to satisfy the constraint at the immersed interface. Moreover, in the FSI setting the projection formulation results in a strongly coupled algorithm that can accurately simulate FSI dynamics involving arbitrarily large structural motions. The governing flow equations are spatially discretized using a nullspace approach that automatically enforces the incompressibility constraint, and when the immersed body is deformable the structural dynamics are spatially discretized using a finite element method. The structural model allows for geometric nonlinearity via a co-rotational formulation. We analytically demonstrate that the proposed time advancement scheme is temporally second order accurate for the primary state variables (e.g., vorticity) and first order accurate for the surface stress. The method is verified using a suite of two-dimensional test problems: flow past both a rigid stationary cylinder at $Re = 200$ and past a deformable flag for various dimensionless parameters. In all cases the results are shown to be in good agreement with the literature.

Acknowledgments

I am deeply grateful for the academic guidance and support offered to me by my advisor, Dr. Andres Goza, whose seemingly endless capacity for patience and compassion allowed me not only to grow and succeed academically, but to enjoy the process while doing it. I found Dr. Goza's excitement for numerical methods, which regularly approached levels of near-giddiness, to be highly contagious. In short order it embedded within me a love for this field that I will surely carry with me for the rest of my life. I would like to further extend my gratitude to my lab mates: Ernold Thompson, Nirmal Nair, and Srikumar Balasubramanian, whose insightful feedback and freely-offered friendship was invaluable both in and outside of the academic setting.

More generally, I would like to thank the greater Aerospace engineering department and the University of Illinois as a whole for providing the environment and resources necessary to make this research possible. In particular I would like to thank Staci McDannel, whose limitless knowledge of the bureaucratic inner-workings of the university combined with her propensity toward helping students at a moment's notice have provided the freedom for me to focus my attention wholly on academic pursuits during my time here.

Finally, I would like to give my warmest thanks to all of my friends and family who have supported me throughout this process: to my parents, for their unfaltering enthusiasm in my work, which remained steadfast even when the details were lost to them; to my partner Caroline, for the countless hours spent graciously listening to me gripe about whatever happened to be the most recent bug plaguing my code; and finally to my brother, who first taught me to love science.

Table of Contents

Chapter 1 Introduction 1

Chapter 2 Governing equations 3
2.1 Fully continuous governing equations 3
2.2 Spatially discrete governing equations 4

Chapter 3 Immersed Boundary Explicit Projection Method . 6
3.1 Runge-Kutta-Chebyshev Method 6
3.2 IBeP method for rigid stationary bodies 8
3.3 IBeP method for FSI problems involving flow past thin deforming bodies 9
3.4 Error scaling of the IBeP Method 11

Chapter 4 Numerical Experiments 13
4.1 Flow past a rigid stationary cylinder 13
4.2 Flapping flag 15

Chapter 5 Conclusions 18

Bibliography 20

Chapter 1

Introduction

The immersed boundary (IB) method is a robust numerical scheme commonly used to solve fluid-structure interaction (FSI) problems. Originally developed by Peskin [1] to simulate blood flow through heart valves, the IB method has since been generalized and adapted by the larger community to simulate a broad range of FSI problems [2]. The utility of the IB method lies in its treatment of the fluid and structure using two separate and independently defined grids. This framework allows for the Navier-Stokes equations to be solved on a standard Eulerian grid, while the potentially time-dependent body positions are treated using a Lagrangian formulation.

When applied to incompressible flows, one of the key bottlenecks to efficient simulations within the IB framework (and more generally) is the treatment of the stiff diffusive term. In order to maintain stability, this term is traditionally treated implicitly in time. When using a fractional step/projection method to advance the system in time, this implicit treatment of the diffusive term nearly always results in a large embedded linear solve within an already large Poisson (or Poisson-like) solve [3–5]. While a variety of efficient techniques have been developed to solve these linear systems, their application in the presence of non-uniform grids and non-standard boundary conditions remains a challenge.

In the present work, we pursue a distinct approach that addresses these challenges by treating the stiff diffusive term with a class of stabilized explicit methods known as super-time-stepping methods. Such methods (which include the Runge-Kutta-Chebyshev (RKC) [6], Runge-Kutta-Legendre (RKL) [7], and Runge–Kutta–Gegenbauer (RKG) [8, 9] methods) are applicable to stiff initial value problems in which the eigenvalues of the Jacobian matrix lie on or very near to the negative real axis, and have been successfully implemented in simulating a wide variety of physical problems [10–15]. Super-time-stepping methods consist of s explicit Runge-Kutta stages, defined such that numerical stability is preserved for time steps on the order of $s^2\Delta t_{exp}$, where Δt_{exp} represents the maximum stable time step of a single stage explicit method.

While super-time stepping methods have been used to stably simulate a wide range of stiff differential equations, less attention has been paid to their development in the differential-algebraic setting relevant to incompressible flows. Recently, Zheng and Petzold [16] extended the RKC method into a projec-

tion method framework with their Runge-Kutta-Chebyshev Projection (RKCP) method. In the RKCP method, the stiff diffusive term of the incompressible Navier-Stokes equations is treated using the RKC method and incorporated into the standard fractional-step approach [17] to project the velocity field onto a divergence-free solution space. To our knowledge, this explicit treatment of the diffusive term has yet to be incorporated into problems in which flow is moving around an immersed body.

In the present work, we derive an RKC-based projection method for problems in which flow is moving past either an arbitrary body undergoing prescribed kinematics, or a thin elastic body whose motion is fully coupled to the flow dynamics (i.e., there is fully coupled fluid-structure interaction). We refer to this proposed method as the immersed boundary explicit projection (IBeP) method. In this method the continuous governing flow equations are spatially discretized using a nullspace approach, so that the Navier-Stokes equations are expressed in a vorticity formulation with the incompressibility constraint automatically enforced [5, 18, 19]. When the immersed body is deformable, the structural equations are discretized using a finite element method, with geometric nonlinearity accounted for via a co-rotational formulation. For both the rigid and thin elastic body scenarios, the stiff diffusive term is treated explicitly in time and the flow stresses on the immersed surface are treated implicitly in time. This formulation utilizes the realization of Taira and Colonius [20] that the surface stresses and no-slip constraint can be cast to fill a mathematically analogous role to the pressure and divergence-free constraint of the incompressible Navier-Stokes equations; i.e., the stresses can be viewed as a Lagange multiplier that is computed to satisfy the algebraic constraint of an index-2 DAE [21]. In this way, the approach described here allows for a robust explicit treatment of the stiff diffusive term while retaining a projection formulation that preserves the no-slip boundary condition to within machine precision. We emphasize that while the presentation below uses the spatially discrete vorticity formulation, an analogous RKC-projection approach can be constructed for a primitive-flow-variable formulation.

This thesis is organized as follows. The governing equations of the immersed boundary projection method are presented in fully continuous and spatially discrete form in chapter 2. In chapter 3 we briefly review the RKC method before presenting the derivation of the IBeP method for stationary rigid bodies and then for deformable surfaces. This is followed by an analytic analysis of the method's order of accuracy. Two 2D numerical simulations are analyzed in chapter 4: flow past an infinite rigid cylinder and flow past a flapping flag. Convergence rate and stability properties are verified, and physical validity of the method is confirmed via comparison against previous experimental and numerical studies. Conclusions are given in chapter 5.

Chapter 2

Governing equations

2.1 Fully continuous governing equations

We consider the nondimensionalized incompressible Navier-Stokes equations defined on a fluid domain $\boldsymbol{\Omega}$ with the Eulerian coordinate $\boldsymbol{x}$ representing position in space:

$$\frac{\partial \boldsymbol{u}}{\partial t} + \boldsymbol{u} \cdot \nabla \boldsymbol{u} = -\nabla p + \frac{1}{Re}\nabla^2 \boldsymbol{u} + \int_{\boldsymbol{\Gamma}} \boldsymbol{f}\left(\boldsymbol{\chi}(\sigma,t)\right) \delta\left(\boldsymbol{\chi}(\sigma,t) - \boldsymbol{x}\right)\, d\sigma \tag{2.1}$$

$$\nabla \cdot \boldsymbol{u} = 0 \tag{2.2}$$

$$\int_{\boldsymbol{\Omega}} \boldsymbol{u}(\boldsymbol{x}) \delta\left(\boldsymbol{x} - \boldsymbol{\chi}(\sigma,t)\right)\, d\boldsymbol{x} = \frac{\partial \boldsymbol{\chi}}{\partial t}. \tag{2.3}$$

The immersed surface, denoted by $\boldsymbol{\Gamma}$, has a position defined by the Lagangrian coordinate $\boldsymbol{\chi}(\sigma,t)$, where σ is a variable that parameterizes the body surface. All spatial variables are nondimensionalized using a characteristic length scale L (e.g., cylinder diameter); The fluid velocity $\boldsymbol{u}$ is nondimensionalized by a characteristic velocity scale U_∞; time t is nondimensionalized by L/U_∞; and pressure and body stress p and $\boldsymbol{f}$, respectively, are nondimensionalized by $\rho_f U_\infty^2$, where ρ_f is the fluid density. The Reynold's number is defined as $Re = U_\infty L/\nu$, where ν represents the fluid kinematic velocity.

The no-slip condition along the immersed surface $\boldsymbol{\chi}$ is enforced by equation (2.3). Analogous to the role of the continuity equation in prescribing pressure, the no-slip constraint is used to compute the surface stress that enforces the no-slip boundary condition on $\boldsymbol{\Gamma}$. Note that the immersed-boundary method used in the present work places fictitious fluid inside of bodies. For thick bodies this yields spurious forces within the body that can artificially contribute to the total stress. Methods have been developed to eliminate this issue [22, 23], though their application in elastic-body FSI settings remains an open research area. We therefore restrict our attention to two configurations in which fictitious fluids intrinsically do not lead to erroneous results: rigid bodies undergoing prescribed motion and thin (i.e., zero internal volume) elastic structures.

2.2 Spatially discrete governing equations

The continuous equations (2.1) to (2.3) are discretized using a standard staggered Cartesian grid finite volume method, as in the formulation of Colonius and Taira [18]:

$$\frac{du}{dt} + \hat{\mathcal{N}}(u) = -Gp + Lu + E^T(\chi) f(t) \tag{2.4}$$

$$Du = 0 \tag{2.5}$$

$$E(\chi) u - \dot{\chi} = 0, \tag{2.6}$$

where u and p denote the spatially discrete velocity and pressure, respectively; $\hat{\mathcal{N}}(u)$ is a function representing a discretization of the nonlinear advection term; and G, L, and D are the discrete gradient, Laplacian, and divergence operators, respectively. The matrix $E(\chi)$ is a discretization of the term involving the delta function in equation (2.3). The discretization of the corresponding term in equation (2.1) is equal to the transpose of E up to a scaling factor of $\Delta s/(\Delta x \Delta y)$, which we absorb into the spatially discrete surface stress f. The convective term is discretized in standard convective form with a central difference approximation of the derivatives, the Laplacian operator is built using the common 5 point finite difference stencil, and G and D are constructed with mimetic finite difference schemes such that $G = -D^T$.

We adopt a nullspace approach in order to eliminate the pressure term and exactly satisfy the continuity equation (2.5), as in Colonius and Taira [18]. Equations (2.4) and (2.5) are transformed to the algebraically equivalent vorticity formulation by the relation $u = C(C^TC)^{-1}\gamma$, where γ represents the discrete vorticity and C is a finite difference approximation to the curl operator defined so that $DC \equiv 0$ (C therefore mimics the property that $\nabla \cdot \nabla \times \boldsymbol{a} \equiv 0$ for any $\boldsymbol{a} \in \mathbb{R}^3$). Using these relations, the spatially discrete equations (2.4) to (2.6) may be rewritten as [18]

$$\frac{d\gamma}{dt} = \mathcal{N}(\gamma) - L\gamma + C^T E^T(\chi) f(t), \tag{2.7}$$

where $\mathcal{N}(\gamma) := -C^T\hat{\mathcal{N}}(C(C^TC)^{-1}\gamma)$. Defining $\zeta := \dot{\chi}$, the spatially discrete equations for flow past a rigid immersed body undergoing prescribed kinematics are written as a system of index-2 differential-algebraic equations (DAEs):

$$\frac{d\gamma}{dt} = \mathcal{N}(\gamma) - L\gamma + C^T E^T(\chi) f(t) \tag{2.8}$$

$$E(\chi)u - \zeta = 0, \tag{2.9}$$

In the setting of the non-rigid FSI problems analyzed in section 4.2, the structural deformations are modeled using a geometrically nonlinear Euler-Bernoulli beam formulation. The beam is spatially discretized using a co-rotational formulation of the finite element method [24] such that numerical accuracy is preserved

in the presence of large displacements and rotations. The discrete beam equation is (nonlinearly) coupled to the discretized Navier-Stokes equations (2.8) and (2.9) to arrive at the spatially discrete, time-continuous FSI equations for flow past a deforming surface:

$$\frac{d\gamma}{dt} = \mathcal{N}(\gamma) - L\gamma + C^T E^T(\chi) f(t) \tag{2.10}$$

$$M\dot{\zeta} + R(\chi) = Q(g + W(\chi) f). \tag{2.11}$$

$$\dot{\chi} = \zeta \tag{2.12}$$

$$E(\chi)u - \zeta = 0, \tag{2.13}$$

In the structural equations (2.11) and (2.12) above, M is a mass matrix; $R(\chi)$ is the internal stress within the body; Qg is a body force term (e.g., gravity); and $QW(\chi) f$ is the stress imposed on the body from the fluid. Refer to Crisfield [24] and Bathe [25] for definitions of the structural matrices and to Goza and Colonius [26] for implementation details associated with the FSI coupling terms. In the present work we restrict ourselves to deformable beams, however, note that equation (2.11) is intentionally written in a generic form valid for a variety of solid materials undergoing large deformations, displacements, and rotations. Thus, while the specific entries in equations (2.11) and (2.12) would vary for other material configurations, these changes would not affect the time-stepping procedure described below.

Chapter 3

Immersed Boundary Explicit Projection Method

In this chapter we present our novel immersed boundary explicit projection method. We begin with a brief review and discussion of the Runge-Kutta-Chebyshev time-stepping method in the differential equation setting in which it was first developed. We then present the IBeP method approach for advancing the spatially discrete governing equations of both rigid bodies undergoing prescribed kinematics (equations (2.8) and (2.9)) and thin elastic bodies coupled to the flow (equations (2.10) to (2.13)). We end the chapter with an analysis of the temporal error scaling of the IBeP method.

3.1 Runge-Kutta-Chebyshev Method

For a moderately stiff ordinary differential equation $\dot{y} = g(y,t)$ with the eigenvalues of the Jacobian Dg restricted near the negative real axis, the RKC algorithm is defined at time t^n as

$$\begin{aligned}
&Y_0 = y(t^n),\\
&Y_1 = Y_0 + \tilde{\mu}_1 \Delta t G_0^n,\\
&Y_j = (1-\mu_j-\nu_j)Y_0 + \mu_j Y_{j-1} + \nu_j Y_{j-2} + \tilde{\mu}_j \Delta t G_{j-1}^n + \tilde{\gamma}_j \Delta t G_0^n, \quad j = 2,\ldots,s,\\
&Y_s = y(t^{n+1}) + \mathcal{O}(\Delta t^3),
\end{aligned} \tag{3.1}$$

where $G_j^n := g(Y_j, t_n + c_j \Delta t)$ and the constant coefficients $\tilde{\mu}_j, \mu_j, \nu_j, \tilde{\gamma}_j$, and c_j are defined using the three-term Chebyshev recursion formula such that accuracy and stability of the method is maintained (see Verwer [27] for details). The region of absolute stability associated with the RKC method encompasses the negative real axis from the origin to a point β, which is given by

$$\beta(s) = (\omega_0 + 1)\frac{T_s''(\omega_0)}{T_s'(\omega_0)} \approx \alpha s^2, \tag{3.2}$$

where the user-specified parameter s is the number of stages, and may be made arbitrarily large to satisfy stability restrictions. The damping parameter ω_0 defines the extent to which the stability region extends into the imaginary plane. The quantities T_s' and T_s'' are the first and second derivatives, respectively, of

the s^{th} Chebyshev polynomial. The scaling factor α is a real-valued constant. The extent of the stability region β is well-suited for treating discretized partial differential equations containing the Laplacian operator, which possesses large negative real eigenvalues. When using a standard uniform grid to define the Laplacian (as is adopted in this work), the eigenvalues are known analytically and the number of stages can be determined as a pre-processing step before the time advancement is performed. We adopt a Newton-Raphson procedure to determine the stages by solving the optimization problem

$$\text{minimize } s \in \mathbb{Z} \text{ subject to } \; |\lambda_{\min}\Delta t| \leq |\beta(s)|\,, \tag{3.3}$$

where $\lambda_{\min}$ is the most negative eigenvalue of the discrete Laplacian operator, given by $\lambda_{\min} = -8/(Re\,\Delta x\Delta y)$ [28]. As can be seen in Figure 3.1, for a typical simulation the number of stages needed to retain stability is small (i.e., less than 10) for any $Re \gtrsim 1$.

This computation of the number of stages reflects the fact that the discrete Laplace operator is the stability bottleneck for the explicit portion of the time advancement. The surface stresses are handled implicitly, and in deforming body FSI problems the structural equations are treated using an implicit Newmark scheme and therefore do not affect stability considerations for the explicitly treated terms.

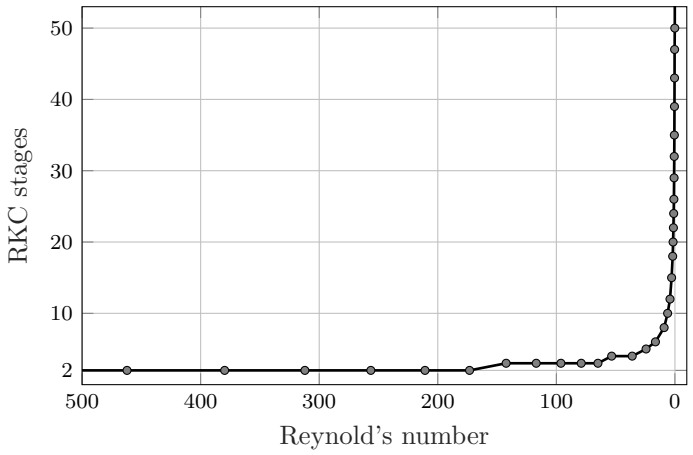

Figure 3.1: Number of RKC stages needed to stably advance in time for various values of Re. Discretization parameters are fixed at $\Delta x = \Delta y = 0.02$ and $\Delta t = 0.01$, which have been arbitrarily chosen to demonstrate the extended stability properties for a typical problem.

In the interest of notational simplicity, we define the operator $\mathcal{R}_s$ to represent the s-stage RKC algorithm in the subsequent sections. Rewriting equation (3.1) in this notation gives

$$y(t^{n+1}) = \mathcal{R}_s\left(G_j^n, y(t^n)\right) + \mathcal{O}(\Delta t^3). \tag{3.4}$$

3.2 IBeP method for rigid stationary bodies

The error analysis in the subsequent section 3.4 will demonstrate that the time advancement scheme requires memory from the surface stress from prior instances to preserve the desired second order accuracy. To motivate this treatment, we Taylor expand the time-dependent surface stress term in equation (2.8) about the solution from the prior time instance:

$$f(t) = f(t^n) + (t - t^n)\dot{f}(t^n) + O(\Delta t^2). \tag{3.5}$$

To within the same order of accuracy in the expansion of $f(t)$, the time rate of change of body stress may be approximated as $\dot{f} = (f(t^{n+1}) - f(t^n))/\Delta t$. Incorporating this approximation into equation (2.8) gives

$$\frac{d\gamma}{dt} = \mathcal{N}(\gamma) - L\gamma + C^T E^T \left(f(t^n) + (t - t^n)\frac{f(t^{n+1}) - f(t^n)}{\Delta t} \right). \tag{3.6}$$

This form of the spatially discrete governing equations may be time-integrated over a time step by treating $\mathcal{N}(\gamma) - L\gamma + \left(1 - \frac{t-t^n}{\Delta t}\right) C^T E^T f(t^n)$ using RKC and analytically integrating the remaining term on the right-hand side, $\frac{t-t^n}{\Delta t} C^T E^T f(t^{n+1})$. The result of this process is

$$\gamma^{n+1} = \mathcal{R}_s(F_j^n, \gamma^n) + \frac{\Delta t}{2} C^T E^T f^{n+1}, \tag{3.7}$$

where $F_j^n := \mathcal{N}(Y_j) - LY_j + (1 - c_j) C^T E^T f^n$. Equation (3.7) is augmented with equation (2.9) (evaluated at the current time step so that the surface stresses may be computed to satisfy the no-slip condition exactly). The aggregate linear system of equations to advance the system in time is ~~therefore~~

$$\begin{bmatrix} I & -C^T E^T \\ EC(C^T C)^{-1} & 0 \end{bmatrix} \begin{bmatrix} \gamma^{n+1} \\ \hat{f}^{n+1} \end{bmatrix} = \begin{bmatrix} \mathcal{R}_s(F_j^n, \gamma^n) \\ \zeta(t^{n+1}) \end{bmatrix}, \tag{3.8}$$

where $\hat{f}^{n+1} = \frac{\Delta t}{2} f^{n+1}$. We adopt the approach of Chang, Giraldo, and Perot [5] to solve this system via a block-LU decomposition. Performing this decomposition on the left-hand side matrix in equation (3.8) and inverting the resulting lower triangular matrix yields the IBeP method for rigid stationary bodies:

$$\gamma^* = \mathcal{R}_s(F_j^n, \gamma^n) \tag{3.9}$$

$$B\hat{f}^{n+1} = -Eu^* + \zeta(t^{n+1}) \tag{3.10}$$

$$\gamma^{n+1} = \gamma^* + C^T E^T \hat{f}^{n+1}, \tag{3.11}$$

where $B = EC(C^T C)^{-1} C^T E^T$ and $u^* = C(C^T C)^{-1}\gamma^*$. The matrix B is small-dimensional (scaling linearly in each dimension with the number of body points along the immersed boundary) and constant in time for a stationary body. Thus, in this case the matrix can be efficiently pre-computed and stored using

a Cholesky decomposition at the start of computation.

Physically, the intermediate vorticity term γ^* in equation (3.9) may be regarded as a solution to the fictitious scenario in which the immmersed body is impulsively removed from the flow field at time t^n. This can be observed in the stage-wise diminishing dependence of F_j^n on the surface stress (in the final stage $c_s = 1$ and therefore the surface stress is removed entirely from computation). In equation (3.10), the stress on the fluid needed for the no-slip constraint to be exactly satisfied is determined, and is then used in equation (3.11) for the projection of the intermediate vorticity onto the solution space that satisfies the requisite boundary condition.

We note that the IBeP method as presented above is highly analogous to the IBP method of Colonius and Taira [18], but with the significant computational advantage of no longer requiring the solution to a large linear system when computing the intermediate flow variable. Moreover, equation (3.10) involves an embedded Poisson problem within B and is therefore well suited to highly tuned solution algorithms, even in the presence of non-uniform and potentially adaptive grids. This outcome is in contrast to prior projection-based immersed boundary methods, in which the embedded linear solve contains additional contributions from the discrete Laplace operator due to the implicit treatment of the diffusive term.

3.3 IBeP method for FSI problems involving flow past thin deforming bodies

The derivation of the IBeP method for coupled FSI problems uses the same temporal discretization of the governing flow equations and no-slip constraint as in section 3.2. The additional equations required to compute the unknown structural motion, equations (2.11) and (2.12), are discretized in time using an implicit Newmark scheme [25]. The resulting algebraic system of equations for the fully coupled FSI system is then

$$\gamma^{n+1} = \mathcal{R}_s(F_j^n, \gamma^n) + C^T {E^{n+1}}^T \hat{f}^{n+1} \tag{3.12}$$

$$\frac{4}{\Delta t^2} M\zeta^{n+1} + \left(R(\chi^{n+1}) + 2QW^{n+1}\hat{f}^{n+1} \right) = r_\zeta^n \tag{3.13}$$

$$\frac{2}{\Delta t}\chi^{n+1} - \zeta^{n+1} = r_\chi^n \tag{3.14}$$

$$E^{n+1}u^{n+1} - \zeta^{n+1} = 0, \tag{3.15}$$

where $r_\zeta^n := M(\frac{4}{\Delta t^2}\chi^n + \frac{4}{\Delta t}\zeta^n + \dot{\zeta^n}) + Qg$, and $r_\chi^n = \zeta^n + \frac{2}{\Delta t}\chi^n$. The notation of the temporal discretization is the same as in Goza and Colonius [26]; see that reference for more details on the various terms. Note that body position and velocity at the current time step have been written as unknown quantities χ^{n+1}

and ζ^{n+1}, respectively, to reflect the fact that they are no longer prescribed quantities in the FSI setting. The interpolation and regularization matrices E and E^T have also been written as E^{n+1} and ${E^{n+1}}^T$, respectively, since they depend on the body position.

The projection approach we employ to simulate the FSI dynamics is analogous to the solution framework for the rigid body setting described in section 3.2. We linearize the system of equations (3.12) to (3.15) and solve the resulting linear system by block-LU factorization. This approach leverages the observation of Goza and Colonius [26] that when the fully discrete FSI equations are linearized about small first order body increments $\Delta\chi$, $\Delta\zeta$ (retaining only first order terms in Δt), the block-LU decomposed equations restrict all iterations for the unknown surface stresses and body motions to small-dimensional subsystems that scale with the number of points on the immersed surface. The key difference in the present approach is that the diffusive term is treated explicitly to avoid additional costly linear solves with the discrete Laplacian operator.

We construct guesses to χ^{n+1} and ζ^{n+1} as $\chi^{n+1}_{(k+1)} = \chi^{n+1}_{(k)} + \Delta\chi$ and $\zeta^{n+1}_{(k+1)} = \zeta^{n+1}_{(k)} + \Delta\zeta$, where the subscript (k) is used to denote the prior guess for the quantity (the solution from time t_n is used as the first guess). An iterative procedure is used to determine solutions for χ^{n+1} and ζ^{n+1} that are converged to within a certain tolerance (determined, for example, by the norm of the increments being sufficiently small). To arrive at a set of equations to solve for the increments $\Delta\chi$ and $\Delta\zeta$, we plug the expressions for $\chi^{n+1}_{(k+1)}$ and $\zeta^{n+1}_{(k+1)}$ into equations (3.12) to (3.15), yielding the linear system

$$\begin{bmatrix} I & 0 & 0 & C^T\left(E^{n+1}_{(k)}\right)^T \\ 0 & 0 & \frac{4}{\Delta t^2}M + \frac{dR}{d\chi}\Big|_{\chi^{n+1}_{(k)}} & 2QW^{n+1}_{(k)} \\ 0 & -I & \frac{2}{\Delta t}I & 0 \\ E^{n+1}_{(k)}C(C^TC)^{-1} & -I & 0 & 0 \end{bmatrix} \begin{bmatrix} \gamma^{n+1} \\ \Delta\zeta \\ \Delta\chi \\ \hat{f}^{n+1}_{(k+1)} \end{bmatrix} = \begin{bmatrix} \mathcal{R}_s(F^n_j, \gamma^n) \\ r^n_\zeta - \frac{4}{\Delta t^2}M\chi^{n+1}_{(k)} - R(\chi^{n+1}_{(k)}) \\ r^n_\chi - \frac{2}{\Delta t}\chi^{n+1}_{(k)} + \zeta^{n+1}_{(k)} \\ \zeta^{n+1}_{(k)} \end{bmatrix}, \tag{3.16}$$

This system can be factorized analogously to the factorization performed on equation (3.8) in the prior section 3.2; i.e., we perform an LU decomposition on the left-hand side matrix of equation (3.16) and invert the resulting lower-triangular matrix to arrive at the IBeP method for deforming surfaces:

$$\gamma^* = \mathcal{R}_s(F^n_j, \gamma^n) \tag{3.17}$$

$$\begin{bmatrix} B^{n+1}_{(k)} & I \\ \frac{4}{\Delta t}QW^{n+1}_{(k)} & \frac{4}{\Delta t^2}M + \frac{dR}{d\chi}\Big|_{\chi^{n+1}_{(k)}} \end{bmatrix} \begin{bmatrix} \hat{f}^{n+1}_{(k+1)} \\ \Delta\zeta \end{bmatrix} = \begin{bmatrix} -E^{n+1}_{(k)}u^* + \zeta^{n+1}_{(k)} \\ \frac{2}{\Delta t}r^\zeta_{(k)} - r^\chi_{(k)} \end{bmatrix} \tag{3.18}$$

$$\Delta\chi = \frac{\Delta t}{2}\left(\Delta\zeta + r^{\chi}_{(k)}\right) \tag{3.19}$$

$$\gamma^{n+1} = \gamma^{*} + C^{T}\left(E^{n+1}\right)^{T}\hat{f}^{n+1}, \tag{3.20}$$

where $B^{n+1}_{(k)} = E^{n+1}_{(k)}C(C^{T}C)^{-1}C^{T}E^{n+1^{T}}_{(k)}$ is the time-varying analog to the B matrix in equation (3.10); $r^{\chi}_{(k)} = r^{n}_{\zeta} - \frac{2}{\Delta t}\chi^{n+1}_{(k)} + \zeta^{n+1}_{(k)}$; and $r^{\zeta}_{(k)} = r^{n}_{\zeta} - \frac{4}{\Delta t^{2}}M\chi^{n+1}_{(k)} - R(\chi^{n+1}_{(k)})$. Note that, as in the rigid body case, the IBeP method for deformable bodies, equations (3.17) to (3.20) is fully explicit in computing the intermediate vorticity, and thereby avoids the large linear solve typically needed due to the implicit treatment of the Laplacian term. We additionally retain the conventional form of the Poisson problem embedded within $B^{n+1}_{(k)}$, without the additional term arising from implicit treatment of the diffusive term that is present in prior projection methods for FSI systems (e.g., in the method of Goza and Colonius [26]). Thus, just as for the rigid body formulation, the proposed IBeP method for FSI systems is well suited to leveraging highly developed solution strategies for solving Poisson problems even in the presence of more complex grid decompositions than are considered here.

3.4 Error scaling of the IBeP Method

In this section we show that the local truncation error in our approximation to $\gamma(t^{n+1})$ and $f(t^{n+1})$ across one time step as computed with the IBeP method scale as $\mathcal{O}(\Delta t^{3})$ and $\mathcal{O}(\Delta t^{2})$, respectively, which implies a global error scaling of $\mathcal{O}(\Delta t^{2})$ in vorticity and $\mathcal{O}(\Delta t)$ in body stress. We consider the case in which the solutions at the start of the time step are known exactly, i.e., $\gamma^{n} = \gamma(t^{n})$ and $f^{n} = f(t^{n})$. It is advantageous to the analysis to define a modified spatially discrete momentum equation,

$$\frac{d\tilde{\gamma}}{dt} = \mathcal{N}(\tilde{\gamma}) - L\tilde{\gamma} + C^{T}E^{T}\left(1 - \frac{t - t^{n}}{\Delta t}\right)f(t^{n}), \tag{3.21}$$

with initial conditions $\tilde{\gamma}(t^{n}) = \gamma(t^{n})$. The difference between $\tilde{\gamma}(t^{n+1})$ and the true solution $\gamma(t^{n+1})$ at the current time step is found by a Taylor series expansion about t^{n}:

$$\gamma(t^{n+1}) - \tilde{\gamma}(t^{n+1}) = \frac{\Delta t}{2}C^{T}E^{T}\left(f(t^{n}) + \Delta t\left.\frac{df}{dt}\right|_{t^{n}}\right) + \mathcal{O}(\Delta t^{3}). \tag{3.22}$$

To leading order in the expansion of equation (3.22), the time rate of change of the surface stress on the righthand side can be approximated as $\dot{f}(t^{n}) = \left(f(t^{n+1}) - f(t^{n})\right)/\Delta t$. This substitution gives

$$\gamma(t^{n+1}) - \tilde{\gamma}(t^{n+1}) = \frac{\Delta t}{2}C^{T}E^{T}f(t^{n+1}) + \mathcal{O}(\Delta t^{3}). \tag{3.23}$$

We can determine $\tilde{\gamma}(t^{n+1})$ to within third order local accuracy in time [29] by applying RKC to equation (3.21). This error scaling of RKC holds in this setting without additional analysis since the modified momentum equation (3.21) is agnostic to the boundary condition (i.e., it is an ordinary differential equation). Applying RKC in this way gives

$$\gamma(t^{n+1}) - \mathcal{R}_s(F_j^n, \gamma^n) = \frac{\Delta t}{2} C^T E^T f(t^{n+1}) + \mathcal{O}(\Delta t^3). \tag{3.24}$$

Multiplying both sides of equation (3.24) by $EC(C^TC)^{-1}$ and using the algebraic constraint equation (2.9) evaluated at the current time step, we compare against equation (3.10) to find

$$f(t^{n+1}) - f^{n+1} = \mathcal{O}(\Delta t^2). \tag{3.25}$$

Substituting this relationship for $f(t^{n+1})$ into equation (3.24) and comparing against equation (3.11) gives the local truncation error in vorticity as

$$\gamma(t^{n+1}) - \gamma^{n+1} = \mathcal{O}(\Delta t^3). \tag{3.26}$$

Thus, the global error of the IBeP method scales as second order in time for vorticity and first order for the surface stresses. For the FSI variant of the algorithm, the novel contribution compared with the IB algorithm of Goza and Colonius [26] is the use of RKC to treat the diffusive term. The manifestation of this treatment is restricted to the governing flow equation and no-slip boundary condition, for which the analysis of this section applies directly. As such, the convergence rate of vorticity and surface stress in equations (3.17) to (3.20) can be inferred to be identical to that of the rigid body case.

We note that the first order scaling in the surface stress is not detrimental to the error scaling of the main quantities of interest (even in the FSI setting where the surface stress is used to update body positions and velocities). However, in certain settings it may be desirable to compute a higher order approximation to the surface stress as a post-processing step. Zheng and Petzold [16] developed a procedure for obtaining a higher order approximation to the pressure for incompressible flows without bodies in a related RKC-projection setting. This approach is based on the improved projection algorithm of Brown, Cortez, and Minion [17] and utilizes information about the time derivative of the divergence constraint. Given the analogous role of the surface stress and no-slip condition to the pressure and divergence-free constraint, a similar procedure could in principle be used to compute higher order approximations to the surface stress, though we leave that direction for future study.

Chapter 4

Numerical Experiments

In this chapter we verify our method by simulating two problems: flow past a rigid stationary cylinder at $Re = 200$ and flow past a deformable flag. For all simulations the multi-domain approach of Colonius and Taira [18] is used, with domains of progressively coarser grid spacing used further from the body. The outermost domain utilizes a zero-Dirichlet boundary condition on the vorticity, and is used to approximate the vorticity boundary conditions at the edges of the finer domains. In all problems analyzed we use equal grid spacing in x and y (i.e., $\Delta x = \Delta y$), and the immersed boundary is discretized as $\Delta s \approx 2\Delta x$, which has been empirically determined to give satisfactory results without allowing for flow permeation through the surface [26, 30]. For all simulations the optimal number of RKC stages is determined automatically at the start of computation by satisfying the optimization equation (3.3). The stage selected by this algorithm retained stability for all cases studied, thereby implicitly verifying the preservation of the extended stability properties of RKC for the DAE projection framework utilized in the IBeP method.

4.1 Flow past a rigid stationary cylinder

We first consider the canonical test case of flow past a spanwise-infinite rigid cylinder of diameter $L = 1$ centered on the origin. To avoid a (singular) impulsive start polluting the temporal convergence rate, incoming flow is smoothly increased from $u = 0$ to $u = U_\infty = 1$ over the first convective time unit. The Reynolds number is fixed at $Re = U_\infty L/\nu = 200$, where ν represents the kinematic viscosity.

For all tests in section 4.1 we compute the flow field on five increasingly coarse domains, the finest being $[-0.5, 3.5] \times [-2.0, 2.0]$ and the largest $[-30.2, 33.2] \times [-31.7, 31.7]$. On the finest grid a spacing of $\Delta x = \Delta y = 0.02$ is used. Early in the simulation a small asymmetric flow perturbation is smoothly introduced to the flow field for a short time in order to initiate vortex shedding. Once the initial transient dynamics have dispersed, the system falls into the familiar periodic vortex shedding pattern of a bluff body. The resultant von Kármán vortex street is shown in the vorticity contour of Figure 4.1. The coefficients of lift and drag, $C_L = 2f_y/\rho U_\infty^2 L$ and $C_D = 2f_x/\rho U_\infty^2 L$, respectively, ($f_x$, f_y is the

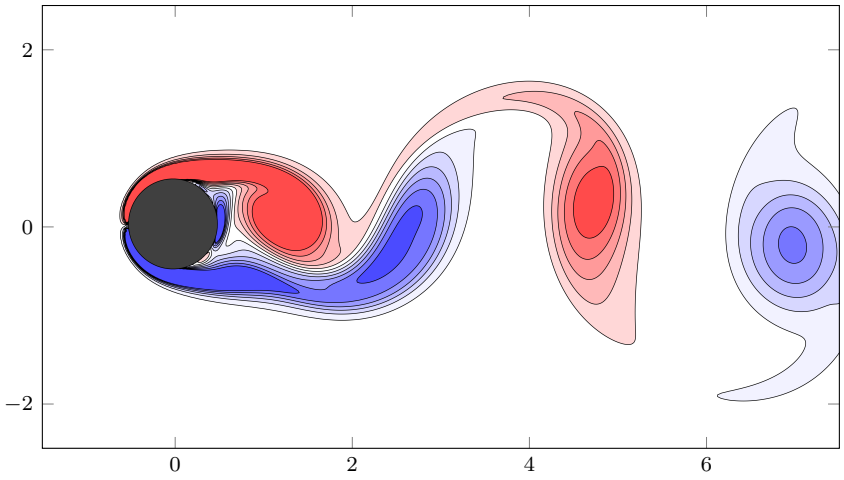

Figure 4.1: Vorticity contour of the von Kármán vortex street observed for flow past a cylinder at $Re = 200$. Contour levels are from -3 to 3 in increments of 1/4.

Study	Strouhal number	Coeff. of lift	Coeff. of drag
Belov et al. [31]	0.193	±0.64	1.19 ± 0.042
Liu et al. [32]	0.192	±0.69	1.31 ± 0.049
Lai and Peskin [33]	0.190		
Roshko [34]*	0.19		
Linnick and Fasel [35]	0.197	±0.69	1.34 ± 0.044
Taira and Colonius [18]	0.195	±0.68	1.34 ± 0.045
Present	0.194	±0.68	1.34 ± 0.044

Table 4.1: Comparison of dimensionless coefficients for flow over cylinder from experimental (denoted by *) and numerical studies at Re = 200.

body stress in the x, y directions) and Strouhal number, $St = L/T_s U_\infty$ (T_s is the vortex shedding period) are compared to previous studies in Table 4.1. All dimensionless coefficients are found to be in good agreement with the literature.

The temporal error scaling of solutions attained at time $t = 1$ by the IBeP method for various time step sizes is shown in Figure 4.2. The spatial grid parameters were kept fixed to the values described above for all trials; these values were selected to produce a spatial error that was much smaller than the temporal error, so that the temporal error was isolated in the convergence studies. The time step was varied logarithmically from $\Delta t_{\min} = 10^{-4}$ to $\Delta t_{\max} = 10^{-2}$. Error in each of these trial solutions was calculated by taking the 2-norm against a fine-time step reference solution obtained using $\Delta t_{\text{fine}} = \Delta t_{\min}/5$. As can be observed in the figure, the error in vorticity and body stress scale in time at the expected convergence rates of $\mathcal{O}(\Delta t^2)$ and $\mathcal{O}(\Delta t)$, respectively.

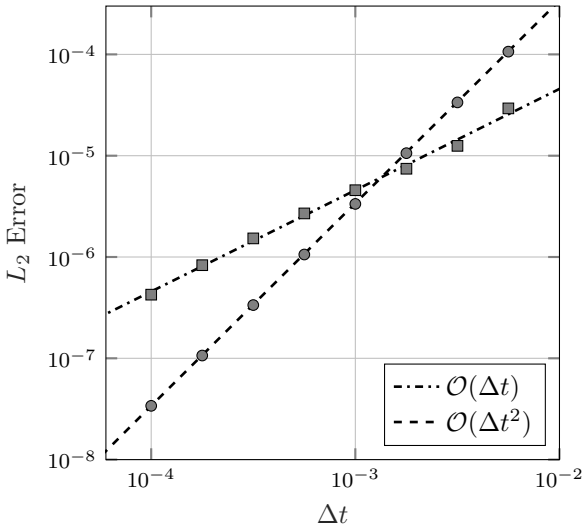

Figure 4.2: Temporal L_2 error in vorticity (●) and body stress (■) for the problem of flow past a stationary cylinder at $Re = 200$.

4.2 Flapping flag

To verify the fully coupled FSI formulation of the IBeP method, we now consider the problem of 2D flow past a deformable flag, represented as a thin geometrically nonlinear Euler-Bernoulli beam with the leading edge pinned at the origin. The incoming flow moves in the $-\hat{y}$ direction. The structural dynamics of the beam are defined by the dimensional parameters of length L, thickness h, solid density ρ_s, and bending stiffness EI. These parameters engender the nondimensional parameters which govern the dynamics of the fully coupled FSI system. These parameters and their definitions are given in Table 4.2. We consider two test cases in which limit-cycle flapping occurs.

Dimensionless parameter	definition	case 1	case 2
Reynolds number (Re)	$U_\infty L/\nu$	1000	200
Mass ratio (M_ρ)	$\rho_s h/\rho_f L$	0.075	1.5
Bending stiffness (K_B)	$EI/\rho_f U_\infty^2 L^3$	10^{-4}	1.5×10^{-3}
Froude number (Fr)	gL/U_∞^2	0.0	0.5

Table 4.2: Dimensionless parameters which govern the dynamics of the flapping beam problem, and their numeric values for the two test cases considered.

In the first test problem the flag was set in a linear initial position in space at an angle of 1° with respect to the $-\hat{y}$ axis. The flow field was computed on five domains, the finest being $[-0.2, 1.8] \times [-0.3, 0.3]$ with a grid spacing of $\Delta x = 0.0025$ and the largest $[-15.20, 16.80] \times [-4.78, 4.78]$. Incoming flow was smoothly increased to $U_\infty = 1$ over the first 0.1 convective time units and a time step of $\Delta t = 0.0006$ was used.

	Study	Amplitude	Flapping frequency
Case 1	Connell and Yue [36]	± 0.096	0.93
	Gurugubelli and Jaiman [37]	± 0.098	0.95
	Goza and Colonius [26]	± 0.097	0.94
	Present	± 0.104	0.95
Case 2	Huang, Shin, and Sung [38]	± 0.35	0.30
	Wang and Eldredge [39]	± 0.35	0.31
	Lee and Choi [40]	± 0.38	0.31
	Goza and Colonius [26]	± 0.38	0.32
	Present	± 0.22	0.33

Table 4.3: Comparison with previous numerical studies of amplitude and frequency associated with the transverse displacement of the beam's trailing edge; obtained for case 1 : ($Re = 1000$, $M_\rho = 0.075$, $K_B = 0.0001$, $Fr = 0$) and case 2 : ($Re = 200$, $M_\rho = 1.5$, $K_B = 0.0015$, $Fr = 1.4$).

For the second case the beam was initially positioned at an angle of 30° with respect to the $-\hat{y}$ axis. A constant gravitational force corresponding to $Fr = 0.5$ was applied to the body in the $-\hat{y}$ direction. The larger mass ratio of this regime provides the inertia necessary for the beam to sustain larger-amplitude flapping relative to that in the first case. We again computed the flow field on five domains, with the finest sub-domain bounded by $[-0.2, 1.8] \times [-0.9, 0.9]$ and discretized by $\Delta x = 0.00625$, and the total domain being of size $[-15.20, 16.80] \times [-7.95, 7.95]$. Incoming flow was smoothly increased to $U_\infty = 1$ over the first 0.1 convective time units and a time step of $\Delta t = 0.0008$ was used.

For both of the test cases considered, the system eventually reaches limit-cycle oscillations of a constant amplitude and frequency in transverse displacement of the trailing edge. Figure 4.3 shows a series of vorticity contour snapshots across one flapping cycle for both cases. The associated amplitude and frequency are tabulated against previous studies in Table 4.3. The results in case 1 agree well with the literature, with flapping frequencies matching to within $\approx 1\%$ and amplitudes to within $\approx 5\%$. While the flapping frequencies agree for case 2, the amplitudes exhibit a significant discrepancy that we attribute to a difference in initial condition: in all studies cited, the flow was impulsively started at the initial time, whereas our simulations smoothly increased flow velocity in order to maintain continuity in the surface stress. The impulsive start introduces significant energy into the system, which would likely lead to the larger-amplitude limit cycle oscillations as observed for the higher-inertia beam of case 2.

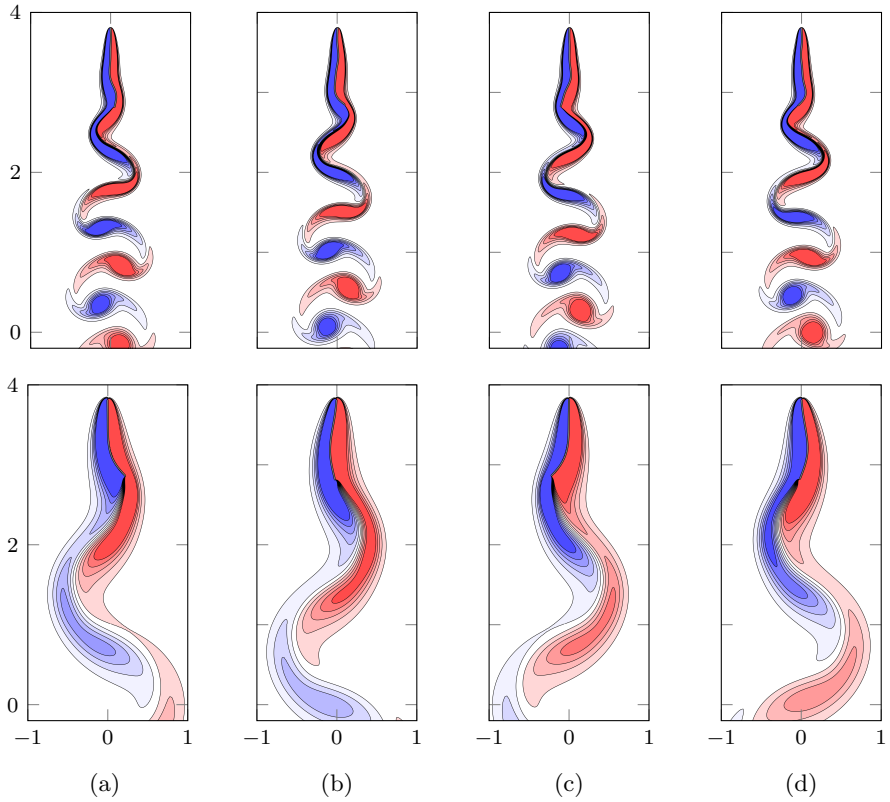

Figure 4.3: Vorticity contours of the limit cycle flapping in case 1 (top row) and case 2 (bottom row) are presented at times (a) $t = 0.25T_s$; (b) $t = 0.5T_s$; (c) $t = 0.75T_s$; and (d) $t = T_s$, where T_s is the period of a single vortex shedding cycle. Contour levels are from -3 to 3 in increments of 1/4.

Chapter 5

Conclusions

We have presented an efficient immersed boundary explicit projection (IBeP) method for problems in which flow is moving past either an arbitrary body undergoing prescribed kinematics, or a thin elastic body whose motion is fully coupled to the flow dynamics. Numerical stability is retained while explicitly advancing the stiff diffusive term by utilizing the extended stability regions of the Runge-Kutta-Chebyshev (RKC) method. At the same time, our approach retains a projection formulation so that the no-slip condition is exactly satisfied at every time instance. In the FSI setting this results in a strongly coupled algorithm that can accurately account for arbitrarily large structural motions. By explicitly advancing the system we avoid the large embedded linear solve within an already large Poisson (or Poisson-like) solve that nearly always arises from implicit treatment of the diffusive term. While a variety of efficient techniques have been developed to solve these large nested linear systems, retaining efficiency of these algorithms remains an open challenge in the presence of non-uniform grids, adaptive grid refinement, non-standard boundary conditions, and parallel processing. By contrast, our explicit treatment of the diffusive term does not suffer from these restrictions and therefore is well-suited to leveraging highly tuned linear solvers, even in the presence of non-uniform grids and for use in tandem with parallel code architectures.

Our formulation utilizes a standard finite volume discretization of the flow equations, cast in a nullspace framework so that the primary flow state variable is the vorticity. This spatial treatment allows for the divergence-free constraint to be automatically satisfied. While we have chosen to employ this spatially discrete vorticity formulation, we emphasize that an analogous RKC-projection approach could be constructed in a primitive-flow-variable formulation, with only relatively superficial changes needed. In the setting of flow past a thin deformable body, a co-rotational beam formulation is used to spatially discretize the structural equations such that arbitrarily large deformations, displacements, and rotations can be accommodated.

Flows past both a rigid stationary cylinder and a flapping flag were simulated using the IBeP method, and in both cases were found to be in good agreement with previous studies. We have shown both analytically and through numerical experiment that the IBeP method retains second order accuracy in flow variables

and first order accuracy in body stress, while preserving the extended stability properties of the RKC method. While not pursued in the present work, it is likely that an additional projection step could be used to raise the convergence rate of the body stress up to second order in time by enforcing the no-slip condition in acceleration. This is analogous to the second order correction step that has been developed for pressure in projection methods outside of the immersed boundary framework.

Bibliography

[1] Charles S Peskin. "Flow patterns around heart valves: A numerical method". In: *Journal of Computational Physics* 10.2 (1972), pp. 252–271.

[2] Rajat Mittal and Gianluca Iaccarino. "Immersed Boundary Methods". In: *Annual Review of Fluid Mechanics* 37.1 (2005), pp. 239–261.

[3] Takeo Kajishima. *Computational Fluid Dynamics Incompressible Turbulent Flows*. eng. 1st ed. 2017. Springer International Publishing : Imprint: Springer, 2017.

[4] Alexandre Joel Chorin. "The numerical solution of the Navier-Stokes equations for an incompressible fluid". In: *Bulletin of the American Mathematical Society* 73.6 (1967), pp. 928–931.

[5] Wang Chang, Francis Giraldo, and J. Perot. "Analysis of an Exact Fractional Step Method". In: *Journal of Computational Physics* 179 (Jan. 2002), pp. 1–17.

[6] B.P. Sommeijer, L.F. Shampine, and J.G. Verwer. "RKC: An explicit solver for parabolic PDEs". In: *Journal of Computational and Applied Mathematics* 88.2 (1998), pp. 315–326.

[7] Chad D. Meyer, Dinshaw S. Balsara, and Tariq D. Aslam. "A stabilized Runge–Kutta–Legendre method for explicit super-time-stepping of parabolic and mixed equations". In: *Journal of Computational Physics* 257 (2014), pp. 594–626.

[8] Stephen O'Sullivan. "Runge–Kutta–Gegenbauer explicit methods for advection-diffusion problems". In: *Journal of Computational Physics* 388 (2019), pp. 209–223.

[9] Timothy Skaras et al. "Super-time-stepping schemes for parabolic equations with boundary conditions". In: *Journal of Computational Physics* 425 (2021), p. 109879.

[10] Ming Chen et al. "An explicit algorithm for modeling planar 3D hydraulic fracture growth based on a super-time-stepping method". In: *International Journal of Solids and Structures* 191-192 (2020), pp. 370–389.

[11] Bhargav Vaidya et al. “Scalable explicit implementation of anisotropic diffusion with Runge–Kutta–Legendre super-time stepping”. In: *Monthly Notices of the Royal Astronomical Society* 472.3 (Aug. 2017), pp. 3147–3160.

[12] Thomas Berlok, Rüdiger Pakmor, and Christoph Pfrommer. “Braginskii viscosity on an unstructured, moving mesh accelerated with super-time-stepping”. In: *Monthly Notices of the Royal Astronomical Society* 491.2 (Nov. 2019), pp. 2919–2938.

[13] R. M. Caplan et al. “Advancing parabolic operators in thermodynamic MHD models: Explicit super time-stepping versus implicit schemes with Krylov solvers”. In: *Journal of Physics Conference Series*. Vol. 837. Journal of Physics Conference Series. May 2017, p. 012016.

[14] D. Barnaś and L.K. Bieniasz. “Utility of super-time-stepping for electroanalytical digital simulations by explicit finite difference methods. Part 2: Spatially two- and three-dimensional models”. In: *Journal of Electroanalytical Chemistry* 838 (2019), pp. 204–211.

[15] Kedar Uprety, Harithar Khanal, and Ananta Upreti. “Super-Time-Stepping Scheme for Option Pricing”. In: *Scientific World* 13.13 (Aug. 2020), pp. 51–54.

[16] Zheming Zheng and Linda Petzold. “Runge–Kutta–Chebyshev projection method”. In: *Journal of Computational Physics* 219.2 (2006), pp. 976–991.

[17] David L. Brown, Ricardo Cortez, and Michael L. Minion. “Accurate Projection Methods for the Incompressible Navier–Stokes Equations”. In: *Journal of Computational Physics* 168.2 (2001), pp. 464–499.

[18] T. Colonius and K. Taira. “A fast immersed boundary method using a nullspace approach and multi-domain far-field boundary conditions”. In: *Computer Methods in Applied Mechanics and Engineering* 197.25-28 (2008), pp. 2131–2146.

[19] Charles Hall. “Numerical Solution of Navier–Stokes Problems by the Dual Variable Method”. In: *SIAM Journal on Algebraic and Discrete Methods* 6 (Apr. 1985).

[20] K. Taira and T. Colonius. “The immersed boundary method: a projection approach”. In: 225.2 (2007), pp. 2118–2137.

[21] R. Glowinski, T.W. Pan, and J. Périaux. “Distributed Lagrange multiplier methods for incompressible viscous flow around moving rigid bodies”. In: *Computer Methods in Applied Mechanics and Engineering* 151.1 (1998). Containing papers presented at the Symposium on Advances in Computational Mechanics, pp. 181–194.

[22] Jeff D. Eldredge. “A method of immersed layers on Cartesian grids, with application to incompressible flows”. In: (In review).

[23] Uğis Lācis, Kunihiko Taira, and Shervin Bagheri. "A stable fluid–structure-interaction solver for low-density rigid bodies using the immersed boundary projection method". In: *Journal of Computational Physics* 305 (2016), pp. 300–318.

[24] M. A. Crisfield. *Non-Linear Finite Element Analysis of Solids and Structures: Essentials*. USA: John Wiley & Sons, Inc., 1991.

[25] K.J. Bathe. *Finite Element Procedures*. Finite Element Procedures pt. 2. Prentice Hall, 1996.

[26] Andres Goza and Tim Colonius. "A strongly-coupled immersed-boundary formulation for thin elastic structures". In: *Journal of Computational Physics* 336 (2017), pp. 401–411.

[27] J.G. Verwer. "Explicit Runge-Kutta methods for parabolic partial differential equations". In: *Applied Numerical Mathematics* 22.1 (1996). Special Issue Celebrating the Centenary of Runge-Kutta Methods, pp. 359–379.

[28] Randall LeVeque. *Finite Difference Methods for Ordinary and Partial Differential Equations: Steady-State and Time-Dependent Problems (Classics in Applied Mathematics Classics in Applied Mathemat)*. USA: Society for Industrial and Applied Mathematics, 2007.

[29] J. G. Verwer, W. H. Hundsdorfer, and B. P. Sommeijer. "Convergence properties of the Runge-Kutta-Chebyshev method". In: *Numerische Mathematik* 57.1 (1990), pp. 157–178.

[30] Bakytzhan Kallemov et al. "An immersed boundary method for rigid bodies". English (US). In: *Communications in Applied Mathematics and Computational Science* 11.1 (2016), pp. 79–141.

[31] A Belov, L Martinelli, and A Jameson. "A new implicit algorithm with multigrid for unsteady incompressible flow calculations". In: *33rd Aerospace Sciences Meeting and Exhibit*.

[32] C. Liu, X. Zheng, and C.H. Sung. "Preconditioned Multigrid Methods for Unsteady Incompressible Flows". In: *Journal of Computational Physics* 139.1 (1998), pp. 35–57.

[33] Ming-Chih Lai and Charles S. Peskin. "An Immersed Boundary Method with Formal Second-Order Accuracy and Reduced Numerical Viscosity". In: *Journal of Computational Physics* 160.2 (2000), pp. 705–719.

[34] Anatol Roshko. "Report 1191: On the development of turbulent wakes from vortex streets". In: (1954).

[35] Mark N. Linnick and Hermann F. Fasel. "A high-order immersed interface method for simulating unsteady incompressible flows on irregular domains". In: *Journal of Computational Physics* 204.1 (2005), pp. 157–192.

[36] Benjamin S. H. Connell and Dick K. P. Yue. “Flapping dynamics of a flag in a uniform stream”. In: *Journal of Fluid Mechanics* 581 (May 2007), p. 33.

[37] P. Gurugubelli and R. Jaiman. “Self-induced flapping dynamics of a flexible inverted foil in a uniform flow”. In: *Journal of Fluid Mechanics* 781 (Oct. 2015), pp. 657–694.

[38] Wei-Xi Huang, Soo Jai Shin, and Hyung Jin Sung. “Simulation of flexible filaments in a uniform flow by the immersed boundary method”. In: *Journal of Computational Physics* 226.2 (2007), pp. 2206–2228.

[39] Chengjie Wang and Jeff D. Eldredge. “Strongly coupled dynamics of fluids and rigid-body systems with the immersed boundary projection method”. In: *Journal of Computational Physics* 295 (2015), pp. 87–113.

[40] Injae Lee and Haecheon Choi. “A discrete-forcing immersed boundary method for the fluid–structure interaction of an elastic slender body”. In: *Journal of Computational Physics* 280 (2015), pp. 529–546.